Materials Advances

ROYAL SOCIETY OF CHEMISTRY

COMMUNICATION

View Article Online
View Journal | View Issue

Cite this: *Mater. Adv.*, 2025, 6, 2154

Received 11th January 2025,
Accepted 24th February 2025

DOI: 10.1039/d5ma00030k

rsc.li/materials-advances

Templating effect travelling on the edge between an ionic liquid and a DES: the case of fluorescent ZnO nanostructures in choline nitrate†

Lorenzo Gontrani, *[a] Lorenzo Casoli, [a] Olga Russina, [b] Elvira Maria Bauer *[c] and Marilena Carbone [a]

In this study, the synthesis and characterization of novel fluorescent ZnO nanopowder are reported. The reaction medium used for the oxide precipitation procedure was choline nitrate, a compound that is a liquid molten salt at room temperature. The purity of the obtained ZnO was assessed through infrared spectroscopy studies and X-ray diffraction analyses; its morphology was observed under SEM, indicating the presence of nanometric spherical aggregates of hexagonal nanocrystals ($d \approx 23$ nm), and the photoluminescence spectrum yielded a broad band in the yellow region (578 nm). All these properties were compared with those of ZnO nanoparticles synthesised in a nitrate-urea deep eutectic solvent, wherein the nanoparticles adopted bidimensional morphology; the XRD spectrum demonstrated a preferential orientation, and the fluorescence peak moved in the orange wavelength range. Thus, we show that the use of urea changes the system from an ionic liquid to a DES and promotes a switch in the template effect from 0D to 2D.

Choline is one of the most important and most studied chemicals in the last decades, as evidenced by the large number of literature references (82 749 items found in a database search performed on Feb 13th, 2025), and its properties span a vast number of disciplines, ranging from medicine to materials science.[1–6] Considering the properties of choline in the latter field, the molecule has proven to be very apt at generating a series of systems with outstanding properties. More specifically, it has been known for quite a long time (since the 1960s) that it can give rise to low melting mixtures when combined with salts of organic acids, such as salicylic acid,[7] a feature that was later exploited by some of us in the preparation of some choline-carboxylate ionic liquids[8] and finally extended to choline-amino acid anion ionic liquids (ChoAA-ILs), whose physical properties (*i.e.* density, viscosity, and refraction index) were thoroughly examined in a study,[9] whereas the structural features of the liquid phase were investigated in a series of non-crystalline X-ray diffraction studies (EDXD).[10–12] The latter class of compounds has proven to be largely harmless[13] and biodegradable,[14,15] possess remarkable solubility properties of lignocellulosic biomasses[16–20] and drugs[21] as well as capture CO_2.[22–24] The properties of choline-based systems are deeply rooted in the manifold intermolecular interactions that the molecule can establish, including "hard" polar interactions between the hydroxyl terminal group (*e.g.* hydrogen bonds) and "softer" ones between the methyl(ammonium) head, which has large extension and consequently low charge density and is polarisable. Depending on the anionic partner, the pool of interactions may result in either high melting-point solids (*e.g.* choline chloride, m.p. = 302 °C) or liquid systems, such as the aforementioned Cho-carboxylates or Cho-AA, and the Cho-nitrate mixture that was employed in the present study. Although the coupling between choline and the small chloride anion is incapable of yielding a liquid system as a consequence of the absence of a "lattice frustration" that is contrariwise experienced when the partners are big and "soft", the presence of this halide anion is crucial for the existence of another family of soft-matter systems recently developed, namely, low melting mixtures known as deep eutectic solvents (DESs). These compounds, which after their discovery in the early 2000s, have progressively become one of the most extensively studied topics of chemical sciences, are characterized by a particularly low melting point owing to the establishment of a wide and diverse network of intermolecular interactions between their constituents, often comprising hydrogen bond acceptors (HBA) and donors (HBD).[25,26] Among all the classes of DESs described in the literature, choline appears as prototype HBA in three of

[a] *STARTNETICS-Department of Chemical Science and Technologies, University of Rome Tor Vergata, Via della Ricerca Scientifica 1, 00133 Rome, Italy. E-mail: lorenzo.gontrani@uniroma2.it*
[b] *Department of Chemistry, Sapienza University of Rome, Piazzale Aldo Moro 5, 00185, Rome, Italy*
[c] *Institute of Structure of Matter-Italian National Research Council (ISM-CNR), c/o Area della Ricerca di Roma1, Strada Provinciale 35d n. 9, Montelibretti, 00010 Rome, Italy. E-mail: elvira.maria.bauer@cnr.it*

† Electronic supplementary information (ESI) available: Rietveld fit of powder XRD spectra, details of the instrumentations used and raw data of XRD, ATR and Fluorescence spectra. See DOI: https://doi.org/10.1039/d5ma00030k

them, while chloride anion often acts as a hub of the interaction network by interacting with choline and HBDs (*e.g.* urea and acids).[27,28] Considering their relatively low toxicity, wide temperature stability, ease of preparation (mixing of the solids and only little heating are required) and high degree of structuring, IL and DES liquid phases have been considered solvents to carry out a large number of chemical reactions in the organic and inorganic domains.[29] In the latter, DESs and ILs have proven to be very effective in the synthesis of metal and metal salt nanoparticles,[30,31] with the added value of imparting specific shapes to the reaction products, profiting from the template effect derived from the microscopic inhomogeneities of the medium. This feature is highly dependent on even small differences under the conditions (type of DES, additives, *etc.*).[32] In our group, the DES approach was recently applied to the synthesis of zinc oxide nanoparticles,[33] obtaining for the first time nanoplatelets (size 10 nm in the shorter, 100 nm in the longer edge) by employing a DES containing hydrated zinc nitrate and urea in 1 : 3.5 and 1 : 7 ratios (liquid around 35–40 °C) as the starting reagent, followed by the precipitation of $Zn(OH)_2$/ZnO after NaOH addition under mild conditions (t = 60 °C).[34] The reaction was partially successful by employing zinc acetate instead of nitrate, but it required higher temperatures. If the reaction is carried out starting from the chloride analogue ($ZnCl_2$: urea DES at the same ratio), nanoparticles of zinc chloride hydroxide monohydrate are obtained. The presence of chloride ions in the zinc salts obtained in the oxide synthesis starting from $ZnCl_2$ with alkali hydroxides as precipitating agents was described in several examples of water-based reactions.[35] Furthermore, in some preliminary studies performed in our lab, it was evidenced that the addition of NaOH to choline chloride:urea 1 : 2 DES containing zinc nitrate led to chloride co-precipitation. The interference of chloride in oxide synthesis may therefore be considered a general limitation. Thus, we attempted to substitute chloride with nitrate, which proved to be a good component when mixed directly with urea, to obtain a chloride:nitrate system (Cho-NO_3) as the starting component, which could possibly be mixed with urea to prepare a DES, in case a liquid phase (of ionic liquid type) was not achieved.

Unfortunately, the literature devoted to the choline:nitrate system is quite scarce. Different procedures were followed to obtain it, and the authors described it sometimes as a solid and some others as a liquid. Following a chronological order, Jia *et al.* in 2014[36] synthesized it by neutralizing a commercial choline hydroxide solution through the dropwise addition of HNO_3 in an ice bath, followed by water removal through distillation and final drying under vacuum; the product was described as an ionic liquid melting at 29 °C and successfully used as battery electrolyte while embedded in chitosan. Later on,[37] Cho-NO_3 was prepared by a metathesis reaction between choline chloride and sodium nitrate in methanol, encompassing the removal of sodium chloride from the reaction mixture. The obtained Cho-NO_3 was dried in an oven under a vacuum at 50 °C for 48 h although it is not stressed too clearly if the salt was liquid or solid because its intended final use was as a water electrolyte solution for supercapacitors, and only the concentration used is reported. In,[38] a similar anion exchange reaction of choline chloride and sodium nitrate was carried out in ethanol by obtaining the "ionic liquid" choline nitrate. Another type of metathesis reaction was performed by Schrade *et al.*,[39] who started from a choline chloride solution, precipitated the chloride as AgCl by adding Ag_2O and treated the filtrate choline hydroxide with HNO_3 until reaching a neutral pH; the mixture did not solidify because the electrolyte solution was the final aim. Alternatively, a DES Cho-NO_3:ethylene glycol starting from the solid salt was employed in a gold electrodeposition study,[40] where the authors prepared it by neutralizing the choline oxide solution with nitric acid; the product was finally "dried under vacuum and recrystallized from absolute ethanol".

In our study, we initially consider the neutralization reaction of choline hydroxide solution (approx. 45 wt%) with nitric acid, but given the large uncertainty about the actual concentration, we preferred to follow the metathesis pathway by dissolving 2.51 g (18 mmol) of choline chloride in the minimum quantity of hot ethanol (around 5 mL) and adding equimolar sodium nitrate (1.523 g) to the mixture. The reaction was conducted in boiling ethanol under reflux at 105 °C for 2 h. At the end, the precipitated solid NaCl was removed from the flask; the liquid phase was first treated using the rotary evaporator at 50 °C and then frozen at −18 °C. An amorphous solid was obtained, which rapidly melted into a viscous brown liquid at room temperature. To remove the interference of ambient humidity and its contamination, the system was freeze-dried at low temperature and pressure (−70 °C and 300 mTorr) and stored in a desiccator. Again, the solid compound turned into a liquid at room temperature; therefore, we decided to use the compound in this form (ionic liquid) without the addition of urea. The liquid was first characterized by infrared spectroscopy (Fig. 1) that confirmed the presence of both choline and nitrate typical vibrational modes and was finally introduced in the reaction round-bottom flask, where two moles of sodium hydroxide per mole of zinc were added under vigorous stirring at 60 °C, as already performed in previous studies in aqueous solutions[34] and nitrate:urea DESs.[33] Quite rapidly, *i.e.* within 5 minutes, the liquid turned into an opalescent white suspension. The sample was illuminated by a portable commercial UV torch (emission maximum around 365 nm) and a bright yellow luminescence could be noticed. After 15 minutes, the vial was removed from the oil bath, and its content was transferred into 20 mL tubes. The milky precipitate (Fig. 1, left panel), slightly

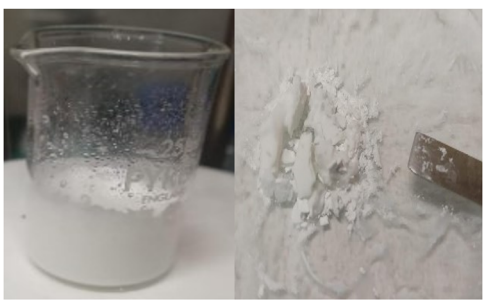

Fig. 1 ZCHNI1 synthesis: precipitate at the end of the reaction in the DES (left) and after water rinsing and drying (right).

fluorescent, was washed with distilled water for a total of 7 rinsing per centrifuge cycles (3500 rpm, 5 min). The pH of the supernatant water was checked at all stages, and the washing procedure terminated when pH 7 was reached, indicating that the surplus of urea and NaOH had been removed. In the final step, the precipitate was centrifuged at a higher speed (4500 rpm), rinsed with ultrapure water, and finally left to dry at 50 °C, leading to a white powder (Fig. 1, right panel), which was called ZCHNI1 (zinc oxide synthesised in choline nitrate). The composition of the choline nitrate intermediate and the synthesised powder was assessed with infrared spectroscopy, obtaining the spectra reported in Fig. 2, where the pattern of solid choline chloride is added for comparison. The analysis of the spectra confirms that the choline nitrate system absorbs large quantities of water immediately after the freeze-drying process, as indicated by the large peak centred at 3380 cm^{-1}, which is attributed to OH-stretching of hydrogen bond water clusters and by the HOH bending peak falling around 1600 cm^{-1}. Moving to lower wavenumbers, the spectrum is dominated by the very intense antisymmetric N–O stretches at ~1370 cm^{-1}, and many other narrower peaks, mostly contributed by choline fragment vibrations, appear in that region. In particular, the comparison with the choline chloride spectrum[41] shows the coincidence between several peaks, notably those at 1479, 1054 and 952 cm^{-1}, ascribable to various CH bending modes. Regarding the spectrum of the solid product, the prominent feature recorded at the rightmost side of the spectrum (peaked at 478 cm^{-1}) can be assigned to Zn–O stretching, and the other shallow peaks at 3300, 1500 and 700 cm^{-1}) may be assigned to vibrational modes of water molecules absorbed on the surface (O–H stretching, O–H bending and L2 librations, respectively,[42] while the absorptions at 1400 and 887 cm^{-1} can be traced back to the stretching and bending of carbonate ions[43] possibly owing to zinc carbonate traces originating from the reaction with atmospheric CO_2. The powder was then investigated with X-ray diffraction. (Fig. 3 and 4c). In the first step, a qualitative comparison with literature database patterns

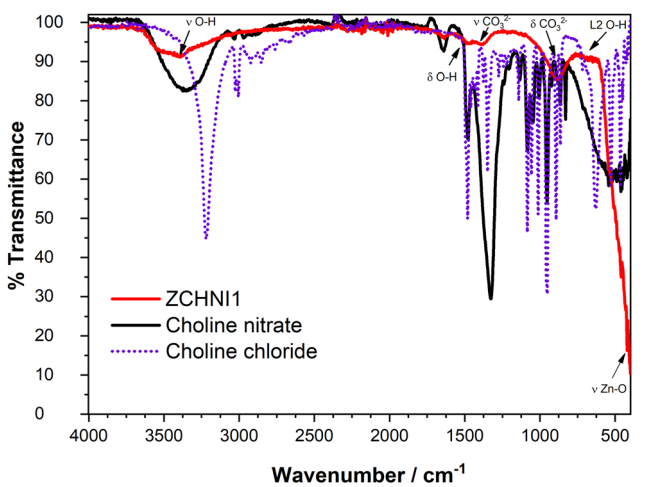

Fig. 2 ATR infrared spectra of the reaction medium (choline nitrate, black), CHNI1 product (ZnO nanoparticles, red) and solid choline chloride (blue dots).

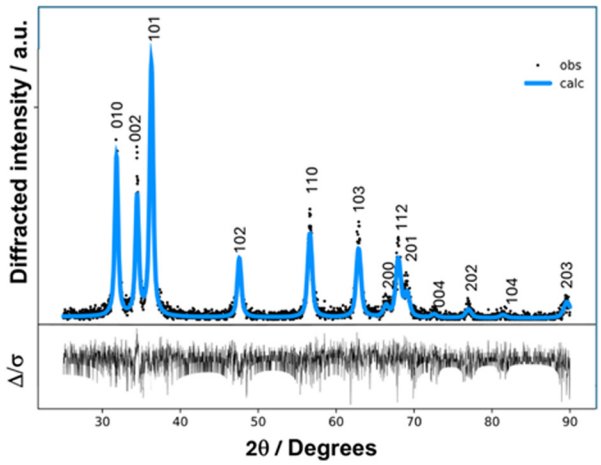

Fig. 3 Power XRD spectrum of ZCHNI1 (black dots) with Rietveld fitting based on ZnO (zincite, cyan line). Vertical digits refer to *hkl* planes of the crystal.

was performed, pointing out that the measured diffraction profile agrees very satisfactorily with the typical triadic fingerprint of Wurtzite-type crystal structures (hexagonal space group $P6_3mc$). In ZnO, this spatial arrangement gives origin to the three easily spottable diffraction signals around 32, 34.5 and 36 degrees, which were observed in the present case at 31.80, 34.47 and 36.29 degrees. These reflections correspond to d-spacings 2.814, 2.602 and 2.475 Å and originate from reflections from 100, 002 and 101 families of crystal planes, respectively. Therefore, the crystallographic data of the zincite mineral (100% ZnO) were employed in the ensuing fitting procedure carried out with the GSAS-II suite of programs.[44] The single-crystal phase data were downloaded from the American Mineralogist crystal structure database with crystallographic information files (CIF) format Mineral.[45] The simulated powder pattern was fitted to experimental data with the Rietveld method in the range of 25-90 degrees, considering that no signals were observed before 30 degrees; by convoluting the reflection peaks, each was modelled as pseudo-Voigt function with asymmetry[46] and using a 3-term Chebyshev polynomial of the first kind as background. The weighted-profile R factor (wR) of the fitting was 29.6%, with χ^2 = 2815 and R = 22.16%. The optimized cell parameters were α,β = 3.256 Å, γ = 5.212 Å, α,β = 90 deg, γ = 120 deg, volume = 47.863 $Å^3$, and density = 5.647 g cm^{-3}; the refined fractional coordinates were Zn 0.333 0.667 −0.022; O 0.333 0.667 0.367. Additionally, the crystallite dimensions were estimated to be in the low nanometric range (fitted value 23.4 nm) according to the Scherrer equation[47] $\sigma = K\lambda/\beta\cos\theta$, which relates the average size σ to the radiation wavelength λ, to the scattering angle θ, and to the half of the maximum intensity (FWMH), denoted as β. Once the composition of the sample had been ascertained, the structural and optical properties of this form of newly synthesized zinc oxide in ionic liquid were compared with those of another type of ZnO recently prepared by our group using zinc nitrate-based DES (code ZND1 = zinc oxide from nitrate DES).[33] In detail, the ZCHNI1 XRD spectrum was compared with that of ZND1 (see ESI,† for details), FE-SEM microscopy studies were carried out to evaluate the morphology of the sample, and

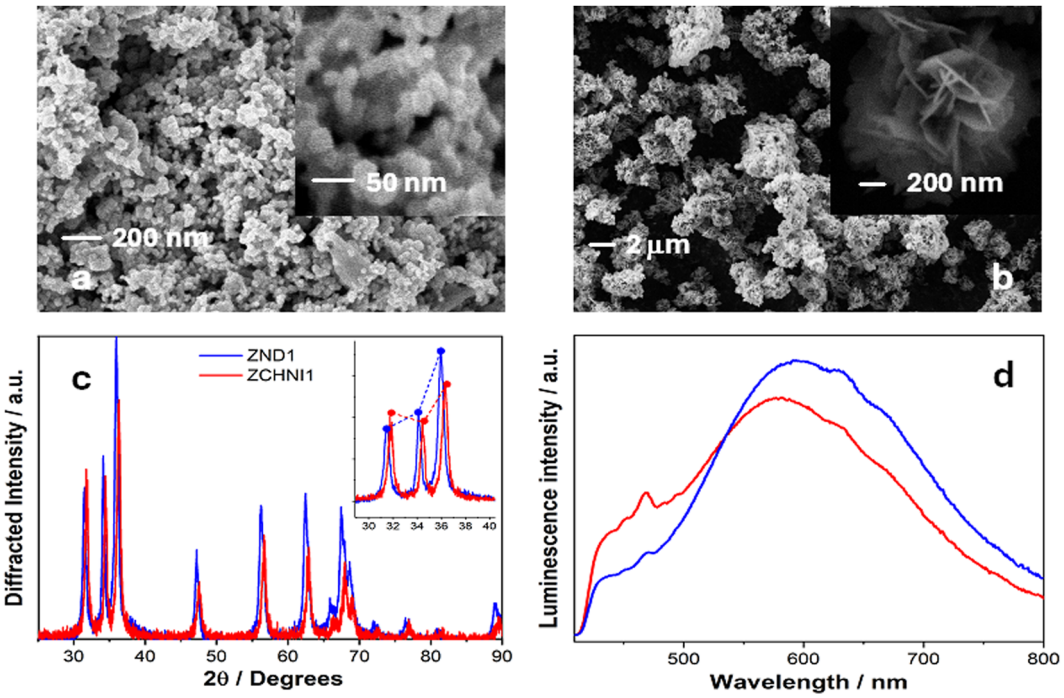

Fig. 4 SEM images of ZCHNI1 (a) and ZND1 (b). Powder XRD (c) and fluorescence spectra (d) of the two samples (ZCHNI1: red; ZND1: blue).

fluorescence measurements were undertaken to investigate the powder photoluminescence. A noteworthy feature of the powder XRD pattern is the presence of a larger significant degree of orientation of the triad peaks in ZND1 compared to ZCHNI1. Indeed, the intensity profile of the triad (medium-low-high) is very similar to the progression observed in bulk crystalline ZnO or in samples composed of spherical nanoparticles,[48] indicating no preferential directions and isotropic crystal growing, while in ZND1, the central peak, relative to the 002 crystal plane, is intermediate and not the lowest peak (see Fig. 4c inset). This anisotropy was quantified in the Rietveld fit using the March-Dollase ratio;[49] additionally, cell dimensions appear slightly enlarged (all diffraction peaks shifted to the left); in particular, the c axis rises to 5.220 Å (see ESI,† for details). The difference in anisotropy predicted by XRD is verified by the analysis of SEM images (Fig. 4a and b), where it can be noticed that ZCHNI1 (Fig. 4a) is composed of nanometric spherical aggregates of pseudo 0D hexagonal nanocrystals (estimated average dimension 43 nm), while in ZND1 (Fig. 4b), flower-like aggregates of 2D pleated nanosheets are found, with only one nanometric lateral dimension (average dimensions: 28 nm (short), 296 nm (long); distance histograms are reported in the ESI†). The different morphologies are reflected in the visible luminescence spectra, as depicted in Fig. 4d. Among the various striking optoelectronic properties of ZnO, its photoluminescence is particularly noticeable because several emission wavelengths can be obtained, some of which show remarkable temperature-dependent features.[50] This behaviour may be explained by the high and varied levels of defectivity in the systems,[51,52] and the strong luminescence observed in the yellow ($\approx$2.0 eV) to red (1.7 eV) regions is linked to oxygen-related defects, including interstitial oxygen and dislocation. In the spectra measured for ZCHNI1 and ZND1 (Fig. 4d) dispersed in ethanol (see ESI,† for further details), it appears clear that the more rounded ZCHNI1 NPs lead to smaller wavelength yellow emission peaked at 578 nm, whereas the longer ZND1 nanosheets (at least in the longitudinal direction) give rise to a stronger orange fluorescence centred at 600 nm. Additionally, both samples share some emission peaklets in the blue-violet range of around 410–430 nm owing to zinc interstitials or vacancies.[51] A naked-eye comparison can be appreciated, as illustrated in Fig. 5, which shows the emission of the two samples (ZCHNI1 on the left side, ZND1 on the right side) in ethanol dispersion (left panel) and as powders (right panel). A plausible explanation for the different morphologies observed can be traced back to the strong templating effect of urea molecules operating in ZND1 synthesis. Despite the apparent geometrical similarities of nitrate anions and urea (both planar trigonal moieties), in the dipolar urea, the highly positive charge density resides on the amino group's side of the

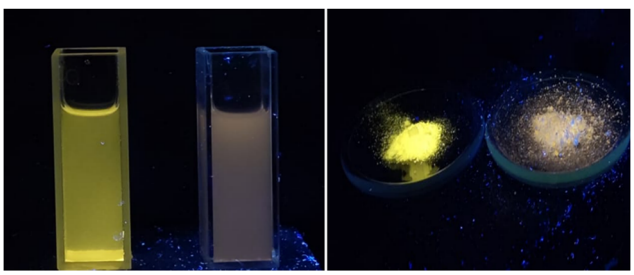

Fig. 5 Luminescence of ethanol dispersions (left panel) and solid powders (right panel). In each picture, ZCHNI1 appears on the left side and ZND1 on the right. The powders were illuminated using a portable UV torch (lamp maximum power at 365 nm).

molecule[53] and favours the deposition of ZnO molecules onto the planar scaffold in a bidimensional fashion, while the nitrate anion is rather "soft" with non-high negative charge density (9 C mm^{-3});[54] a similar low charge density and isotropic structuring behaviour may be hypothesised for the bulky and highly polarisable choline cation so that the choline + nitrate combination does not impart topological bias to the diffusion of zinc and hydroxide ions in the liquid. Conversely, urea produces a marked structural ordering, resulting in the observed planar templating effect; this ordering was experimentally observed in neutron diffraction studies of choline chloride-urea 1:2 deep eutectic solvent liquid phase (reline).[28] A comparable templating effect involving the establishment of an ordered mesoscopic phase was recognized in some other inorganic materials, such as the sheet-like cuprous oxide nanoparticles obtained in water solutions with added polymers (see Fig. 9 of ref. 55 and ref. 56).

Conclusions

In summary, this contribution sheds light on how it is possible to easily synthesise nanometric ZnO powders of spherical morphology with a choline nitrate ionic liquid and describes how the nanomorphology can be tuned from 0D to 2D by substituting the choline cation with urea in the reaction mixture, which changes from ionic liquid to DES. Further studies on other quaternary ammonium ionic liquids and DES are underway to corroborate our hypothesis.

Author contributions

Lorenzo Gontrani: writing – original draft, writing – review and editing, conceptualization, and investigation. Lorenzo Casoli: investigation and visualization, Olga Russina: investigation and resources. Elvira M. Bauer: investigation and data curation. Marilena Carbone: writing – review and editing, validation, supervision, and project administration.

Data availability

The data supporting this article have been included as part of the ESI.† Crystallographic data are available from the databases cited in the references.

Conflicts of interest

There are no conflicts to declare.

Acknowledgements

L. G, M. C. and E. M. B. acknowledge GREEN3 (CUP E53D23005230006; project number: 2022F4YZP9) project funded by the Ministero dell'Università e della Ricerca within the PRIN 2022 program and the support from the Project X-CHEM under the MUR program "Dipartimenti di Eccellenza 2023–2027" (CUP E83C23000340006).

Notes and references

1 Y. Yao, Z. Ye, Y. Zhang, Y. Wang and C. Yu, *Adv. Mater. Interfaces*, 2024, **11**, 2300946.
2 S. Kliewer, S. G. Wicha, A. Bröker, T. Naundorf, T. Catmadim, E. K. Oellingrath, M. Rohnke, W. R. Streit, C. Vollstedt, H. Kipphardt and W. Maison, *Colloids Surf B Biointerfaces*, 2020, **186**, 110679.
3 G. Acik, *React. Funct. Polym.*, 2021, **168**, 105035.
4 S. H. Zeisel, D. Char and N. F. Sheard, *J. Nutr.*, 1986, **116**, 50–58.
5 T. Yang, Y. Nian, H. Lin, J. Li, X. Lin, T. Li, R. Wang, L. Wang, G. A. Beattie, J. Zhang and M. Fan, *Sci. Adv.*, 2024, **10**(33), eado6229.
6 S. H. Zeisel and K.-A. da Costa, *Nutr. Rev.*, 2009, **67**, 615–623.
7 K. B. Wróblewska, S. Plewa, P. Dereziński and I. Muszalska-Kolos, *Molecules*, 2019, **25**, 51.
8 L. Tanzi, F. Ramondo, R. Caminiti, M. Campetella, A. Di Luca and L. Gontrani, *J. Chem. Phys.*, 2015, **143**, 114506.
9 S. De Santis, G. Masci, F. Casciotta, R. Caminiti, E. Scarpellini, M. Campetella and L. Gontrani, *Phys. Chem. Chem. Phys.*, 2015, **17**, 20687–20698.
10 M. Campetella, D. C. Martino, E. Scarpellini and L. Gontrani, *Chem. Phys. Lett.*, 2016, **660**, 99–101.
11 M. Campetella, S. De Santis, R. Caminiti, P. Ballirano, C. Sadun, L. Tanzi and L. Gontrani, *RSC Adv.*, 2015, **5**, 50938–50941.
12 S. Di Muzio, O. Russina, D. Mastrippolito, P. Benassi, L. Rossi, A. Paolone and F. Ramondo, *J. Mol. Liq.*, 2022, **352**, 118427.
13 S. Zhang, L. Ma, P. Wen, X. Ye, R. Dong, W. Sun, M. Fan, D. Yang, F. Zhou and W. Liu, *Tribol Int.*, 2018, **121**, 435–441.
14 A. Yazdani, M. Sivapragasam, J. M. Leveque and M. Moniruzzaman, *J. Microb. Biochem. Technol.*, 2016, **08**, 4015–4021.
15 S. H. Baharuddin, N. A. Mustahil, A. A. Abdullah, M. Sivapragasam and M. Moniruzzaman, *Procedia Eng.*, 2016, **148**, 401–408.
16 X.-D. Hou, N. Li and M.-H. Zong, *ACS Sustainable Chem. Eng.*, 2013, **1**, 519–526.
17 P. Reddy, *S Afr. J. Sci.*, 2015, **111**, 9.
18 R. Wang, Y. Chang, Z. Tan and F. Li, *Sep. Sci. Technol.*, 2016, **51**, 1093–1102.
19 T. Q. To, K. Procter, B. A. Simmons, S. Subashchandrabose and R. Atkin, *Faraday Discuss.*, 2018, **206**, 93–112.
20 Q.-P. Liu, X.-D. Hou, N. Li and M.-H. Zong, *Green Chem.*, 2012, **14**, 304–307.
21 M. A. Alawi, I. I. Hamdan, A. A. Sallam and N. A. Heshmeh, *J. Mol. Liq.*, 2015, **212**, 629–634.
22 L. Zhang, J. Wang, Z. Liu, Y. Lu, G. Chu, W. Wang and J. Chen, *AIChE J.*, 2013, **59**, 2957–2965.
23 S. Bhattacharyya and F. U. Shah, *ACS Sustainable Chem. Eng.*, 2016, **4**, 5441–5449.
24 V. B. Saptal and B. M. Bhanage, *ChemSusChem*, 2017, **10**, 1145–1151.
25 D. O. Abranches and J. A. P. Coutinho, *Curr. Opin. Green Sustainable Chem.*, 2022, **35**, 100612.
26 B. B. Hansen, S. Spittle, B. Chen, D. Poe, Y. Zhang, J. M. Klein, A. Horton, L. Adhikari, T. Zelovich, B. W. Doherty, B. Gurkan, E. J. Maginn, A. Ragauskas, M. Dadmun,

T. A. Zawodzinski, G. A. Baker, M. E. Tuckerman, R. F. Savinell and J. R. Sangoro, *Chem. Rev.*, 2021, **121**, 1232–1285.
27 L. Gontrani, N. V. Plechkova and M. Bonomo, *ACS Sustainable Chem. Eng.*, 2019, **7**, 12536–12543.
28 O. S. Hammond, D. T. Bowron and K. J. Edler, *Green Chem.*, 2016, **18**, 2736–2744.
29 F. M. Perna, P. Vitale and V. Capriati, *Curr. Opin. Green Sustainable Chem.*, 2020, **21**, 27–33.
30 L. Gontrani, P. Tagliatesta, D. T. Donia, E. M. Bauer, M. Bonomo and M. Carbone, *Molecules*, 2022, **27**, 2045.
31 D. V. Wagle, H. Zhao and G. A. Baker, *Acc. Chem. Res.*, 2014, **47**, 2299–2308.
32 H. Liao, Y. Jiang, Z. Zhou, S. Chen and S. Sun, *Angew. Chem., Int. Ed.*, 2008, **47**, 9100–9103.
33 L. Gontrani, D. T. Donia, E. Maria Bauer, P. Tagliatesta and M. Carbone, *Inorg. Chim. Acta*, 2023, **545**, 121268.
34 D. T. Donia, E. M. Bauer, M. Missori, L. Roselli, D. Cecchetti, P. Tagliatesta, L. Gontrani and M. Carbone, *Symmetry*, 2021, **13**, 733.
35 A. Driot and C. R. Hebd, *Seances Acad. Sci.*, 1910, **150**, 1426–1428.
36 X. Jia, Y. Yang, C. Wang, C. Zhao, R. Vijayaraghavan, D. R. MacFarlane, M. Forsyth and G. G. Wallace, *ACS Appl. Mater. Interfaces*, 2014, **6**, 21110–21117.
37 P. Przygocki, Q. Abbas, B. Gorska and F. Béguin, *J. Power Sources*, 2019, **427**, 283–292.
38 M. Jafari and A. Heydari, *J. Mol. Struct.*, 2022, **1264**, 133267.
39 S. Schrade, Z. Zhao, Z. Supiyeva, X. Chen, S. Dsoke and Q. Abbas, *Electrochim. Acta*, 2022, **425**, 140708.
40 T. Geng, B. W. Schick, M. Uhl, A. J. C. Kuehne, L. A. Kibler, M. U. Ceblin and T. Jacob, *ChemElectroChem*, 2022, **9**, e202101263.
41 M. A. Ali, M. A. Kaium, S. N. Uddin, M. J. Uddin, O. Olawuyi, A. D. Campbell, C. J. Saint-Louis and M. A. Halim, *ACS Omega*, 2023, **8**, 38243–38251.
42 G. R. Medders and F. Paesani, *J. Chem. Theory Comput.*, 2015, **11**, 1145–1154.
43 Y. Kim, M.-C. Caumon, O. Barres, A. Sall and J. Cauzid, *Spectrochim Acta A Mol Biomol Spectrosc*, 2021, **261**, 119980.
44 B. H. Toby and R. B. Von Dreele, *J. Appl. Crystallogr.*, 2013, **46**, 544–549.
45 R. T. Downs and M. Hall-Wallace, *Am. Mineral.*, 2003, **88**, 247–250.
46 L. W. Finger, D. E. Cox and A. P. Jephcoat, *J. Appl. Crystallogr.*, 1994, **27**, 892–900.
47 A. L. Patterson, *Acta*, 1939, **56**, 978–982.
48 C. F. Holder and R. E. Schaak, *ACS Nano*, 2019, **13**, 7359–7365.
49 E. Zolotoyabko, *J. Appl. Crystallogr.*, 2009, **42**, 513–518.
50 R. L. D'Amato, in preparation.
51 R. Crapanzano, I. Villa, S. Mostoni, M. D'Arienzo, B. Di Credico, M. Fasoli, R. Scotti and A. Vedda, *Nanomaterials*, 2020, **10**, 1983.
52 H. Zeng, G. Duan, Y. Li, S. Yang, X. Xu and W. Cai, *Adv. Funct. Mater.*, 2010, **20**, 561–572.
53 J.-C. Liu and G.-Z. Jia, *J. Solution Chem.*, 2016, **45**, 485–496.
54 R. D. Shannon, *Acta Crystallogr., A*, 1976, **32**, 751–767.
55 Y. Xie, D. Kocaefe, C. Chen and Y. Kocaefe, *J. Nanomater.*, 2016, **2016**, 1–10.
56 L. Ru, Y. Liang-Min, J. Lan-Ni, Y. Xue-Feng and D. Lei, *Chin. J. Inorg. Chem.*, 2013, **29**, 265–270.